Diamagnetism, transport, magnetothermoelectric power, and magnetothermal conductivity in electron-doped CaMn$_{1-x}$V$_x$O$_3$ manganites

R. Ang,[a] Y. P. Sun,[a,b] Y. Q. Ma, B. C. Zhao, X. B. Zhu, and W. H. Song

Key Laboratory of Materials Physics, Institute of Solid State Physics, Chinese Academy of Sciences, Hefei 230031, People's Republic of China and Hefei High Magnetic Field Laboratory, Chinese Academy of Sciences, Hefei 230031, People's Republic of China

The effects of V doping on field-cooled magnetization $M_{FC}(T)$, zero-field-cooled magnetization $M_{ZFC}(T)$, resistivity ρ, thermoelectric power S, and thermal conductivity κ in manganites CaMn$_{1-x}$V$_x$O$_3$ ($0.02 \leqslant x \leqslant 0.08$) have been investigated systematically. As the V doping level exceeds 0.02, an anomalous "diamagnetism" has been observed. It is suggested that the force generated by the orbit rotation of e_g electron in Mn^{3+}O$_6$ octahedron makes the spin tilt, as a result, the vector sum of individual spins may be along or opposite to the direction of the applied magnetic field, and macroscopically, the average magnetization exhibits positive or negative values. In addition, the transport mechanism in the high and low temperature ranges is dominated by the small polaron conduction and the variable-range-hopping conduction, respectively, according to the fitting analysis of the temperature dependence of Seebeck coefficient $S(T)$ and resistivity $\rho(T)$. Both S and κ peaks appearing at low temperature is gradually suppressed by V doping. Additionally, obvious magnetothermoelectric power and magnetothermal conductivity are observed in the temperature region which an anomalous diamagnetism appears. The results are discussed based on spin-orbital coupling and spin-phonon coupling induced due to V doping, respectively. Moreover, the large thermoelectric figure of merit $Z = S^2/\rho\kappa$ for the slightly V-doped sample suggests that the V-doped manganite may be a good candidate for thermoelectric materials. © *2006 American Institute of Physics*. [DOI: 10.1063/1.2337557]

I. INTRODUCTION

The hole-doped (Mn^{3+}-rich) manganites $R_{1-x}A_x$MnO$_3$, where R stands for a trivalent rare earth such as La, Pr, Nd, etc., and A represents a divalent alkaline earth such as Ca, Sr, Ba, etc., have received considerable attention in recent years due to the discovery of colossal magnetoresistance (CMR) and more generally because of the unusually strong coupling among their charge, spin, orbit, and lattice degrees of freedom.[1] Their behavior has been interpreted based on the double-exchange (DE) mechanism[2] and the Jahn-Teller (JT) distortion.[3,4] At present, the polarons are also extensively invoked to explain the magnetoresistance (MR) properties of manganites.[5]

In contrast to the hole-doped manganites, the electron-doped (Mn^{4+}-rich) manganites have also been widely studied due to the potential applications in the field of spintronics. In the electron-doped manganites LMnO$_3$ (L=La, Ca, etc.) system, one efficient way to induce CMR is the substitution of L site such as La$_{1-x}$(Ce,Zr,Te)$_x$MnO$_3$,[6] Ca$_{1-x}$(Bi,Eu,Sm)$_x$MnO$_3$,[7] etc., which has stirred up interest due to the MR effects. The other way is doping the Mn site with the cations having a valency larger than that of Mn^{4+}. It is believed that the study of the doping effects at Mn site should provide important clues to the mechanism of CMR

behavior because of the core role of Mn ions, which is supported by the recent research work in the doped manganites CaMn$_{1-x}$M$_x$O$_3$ with M=Nb, Ta, W, Mo, Re, and Ru.[8]

Among the investigation of all Mn-site doping, the V doping is more interesting because of its special nature of V ions. In V-based oxides such as LaVO$_3$ and YVO$_3$, which gives rise to an anomalous "diamagnetism,"[9] and V^{3+} ion with a localized $3d^2$ configuration plays a key role in the diamagnetism of LaVO$_3$. As to V^{5+} ion, which itself with empty $3d$ orbits exhibits an orbital diamagnetism. Due to the nature of V ions, here, we report the observation of diamagnetism in V-doped $3d^3$ system CaMnO$_3$.

In this paper, we analyze the origin of diamagnetism in detail. We have also investigated the effects of V doping at the Mn site of CaMnO$_3$ using thermoelectric power (TEP) S and thermal conductivity κ measurements. Unlike resistivity ρ, S is a zero-current transport coefficient which can reflect the intrinsic properties of the sample without being affected by grain boundaries. In addition, S is very sensitive to the band structure and carrier mobility near the Fermi level, which can be used to clarify the electronic structure in the different phases of CaMn$_{1-x}$V$_x$O$_3$. In order to investigate the transport mechanism and understand fully the origin of the effect of V doping at Mn sites, in this paper, the effect of V doping at Mn site on field-cooled (FC) magnetization M_{FC}, zero-field-cooled (ZFC) magnetization M_{ZFC}, ρ, S, and κ of CaMn$_{1-x}$V$_x$O$_3$ ($0.02 \leqslant x \leqslant 0.08$) has been systematically studied.

[a] Electronic mail: rang@issp.ac.cn
[b] Author to whom correspondence should be addressed; Fax: +86-551-559-1434; electronic mail: ypsun@issp.ac.cn

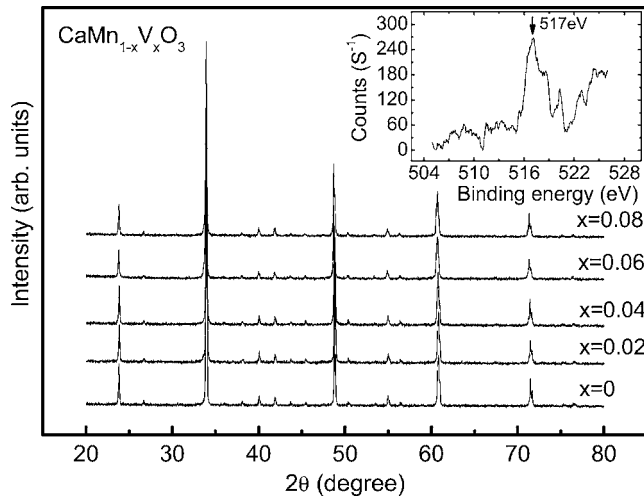FIG. 1. X-ray diffraction patterns of $CaMn_{1-x}V_xO_3$ (x=0, 0.02, 0.04, 0.06, and 0.08) samples at room temperature. The inset shows the XPS spectrum corresponding to vanadium $2p_{3/2}$.

II. EXPERIMENT

A series of polycrystalline samples of $CaMn_{1-x}V_xO_3$ (x =0.02, 0.04, 0.06, and 0.08) was prepared from $CaCO_3$, V_2O_3, and Mn metal by a citrate gel technique. Stoichiometric amounts of the starting materials were dissolved in diluted nitric acid (HNO_3) to which was added an excess of citric acid and ethylene glycol to make a metal complex. After all the reactants had completely dissolved, the solution was mixed and heated on a hot plate resulting in the formation of a gel. The gel was dried at 250 °C, and then heated to 600 °C to decompose the nitrates and to remove the organic. The resulting powder was pressed into pellets, each of which was sintered at 1100 °C for 48 h with an intermediate regrinding again, and finally, the furnace was cooled down to room temperature. The sample $CaMnO_3$ was prepared by the conventional solid state reaction method.

X-ray diffraction (XRD) patterns of all the samples were obtained on a Philips diffractometer with Cu $K\alpha$ radiation at room temperature. X-ray photoelectron spectroscopy (XPS) measurement was performed on ESCALAB MK-II (UK) spectrometer. The magnetic measurements were performed on a Quantum Design superconducting quantum interference device (SQUID) magnetic property measurement system (MPMS) ($2 \leqslant T \leqslant 400$ K, $0 \leqslant H \leqslant 5$ T) with ultralow field option. The temperature dependence of $\rho(T)$, $S(T)$, and $\kappa(T)$ was measured by a standard four-probe method in a commercial Quantum Design physical property measurement system (PPMS) ($1.8 \leqslant T \leqslant 400$ K, $0 \leqslant H \leqslant 9$ T), respectively. The typical dimension of the measured sample is $8 \times 4 \times 1.2$ mm³.

III. RESULTS AND DISCUSSION

A. Structure of $CaMn_{1-x}V_xO_3$

The powder x-ray diffraction of $CaMn_{1-x}V_xO_3$ samples ($0 \leqslant x \leqslant 0.08$) at room temperature is shown in Fig. 1. It indicates that all samples are single phase with no detectable secondary phases and the samples have an orthorhombic structure with the space group *Pnma*. The Mn valence (δ) in
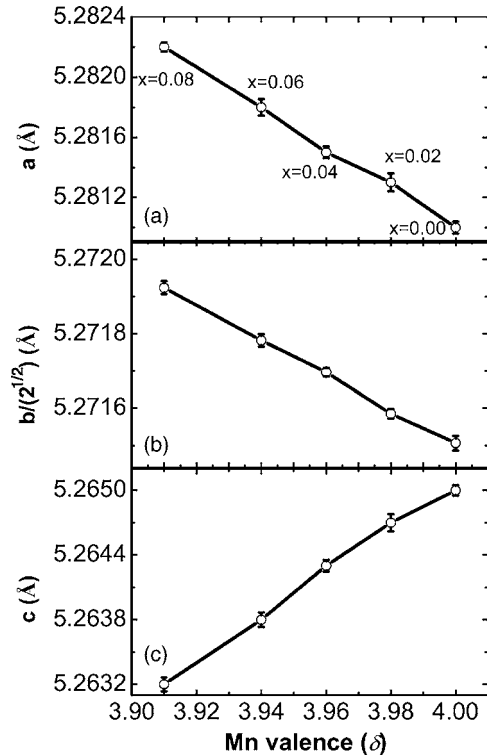

FIG. 2. Mn valence dependence of the lattice parameters (a, b/$\sqrt{2}$, c). The solid line is only guide to the eyes.

$CaMn_{1-2x}^{4+}Mn_x^{3+}V_x^{5+}O_3$ system is calculated according to the relation $\delta=(4-5x)/(1-x)$. The δ dependence of the lattice parameters ($a,b/\sqrt{2},c$) is shown in Figs. 2(a)–2(c), respectively. It is clearly shown that the perovskite cell belongs to O type, which is $a>b/\sqrt{2}>c$, i.e., without the cooperative JT effect due to the separate local JT distortion each other.

B. Valence of vanadium

The inset of Fig. 1 shows the XPS measurement on the $CaMn_{0.96}V_{0.04}O_3$ sample to confirm the valency of vanadium. The spectrum was recorded in the binding energy range of 505–526 eV. A peak (after subtraction of an oxygen O_{1s} satellite peak) corresponding to vanadium $2p_{3/2}$ locates at binding energy of 517 eV, which is in good agreement with the result reported in V_2O_5, indicating that the valence of V is +5.[10]

C. Magnetic property

The temperature dependence of FC and ZFC magnetizations $M_{FC}(T)$ (solid circles) and $M_{ZFC}(T)$ (empty circles) measured in an applied magnetic field of H=0.01 T for all $CaMn_{1-x}V_xO_3$ samples is shown in Fig. 3. The magnetic transition temperatures T_m, defined as the temperature where $|dM/dT|$ is maximum, for each sample are 121, 118, 111, 99, and 102 K, respectively. For the free sample, $M_{ZFC}(T)$ and $M_{FC}(T)$ curves disperse below $T_m \sim 121$ K. The $M_{ZFC}(T)$ and $M_{FC}(T)$ curves of $CaMn_{0.98}V_{0.02}O_3$ as plotted in Fig. 3(a) exhibit small difference compared with the other samples and show two transitions around temperatures of 54 and 118 K. The magnetic behavior between these two temperatures can be attributed to the competition between the DE
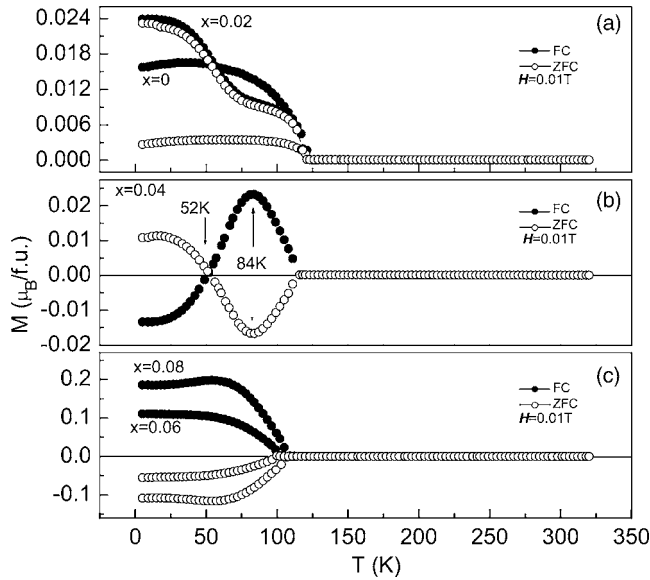
FIG. 3. The temperature dependence of field-cooled and zero-field-cooled magnetizations M_{FC} (solid circles) and M_{ZFC} (empty circles) measured in an applied magnetic field of $H=0.01$ T for all the samples.
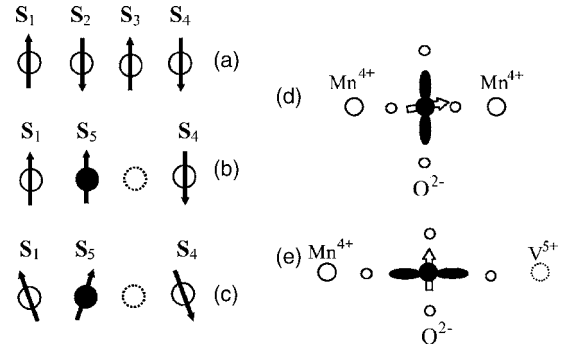

FIG. 4. Schematic spin configurations. In (a), a G-type AFM structure of localized spins of Mn^{4+} ions (○) in $CaMnO_3$ is shown. (b) shows the spin configuration after V^{5+} (⊙) doping. Symbol (●) denotes Mn^{3+} ion. (c) shows the possible canted spin structure in $CaMn_{1-x}V_xO_3$. The illustration for the $Mn^{3+}O_6$ octahedron distortion due to (d) Jahn-Teller effect and (e) V^{5+} substitution for Mn^{4+}.

ferromagnetism (FM) interaction of $Mn^{3+}-O-Mn^{4+}$ and superexchange antiferromagnetism (AFM) interaction of $Mn^{4+}-O-Mn^{4+}$.

Figure 3(b) shows the $M_{FC}(T)$ and $M_{ZFC}(T)$ curves of $CaMn_{0.96}V_{0.04}O_3$. With decreasing temperature below T_m, M_{FC} first increases, reaching a maximum at 84 K, and then decreases continuously, crossing zero at 52 K to negative values, which is referred to as the diamagnetism below for convenience. $M_{ZFC}(T)$ pattern below T_m seems to be a mirror image of $M_{FC}(T)$ curve, and has nearly the same compensation point corresponding $M=0$ at 52 K. For the sample with $x=0.06$ as shown in Fig. 3(c), $M_{FC}(T)$ shows a magnetic transition at 99 K, below which it monotonously decreases with increasing temperature from 5 K without the appearance of negative M values. In opposite to $M_{FC}(T)$, $M_{ZFC}(T)$ below 99 K keeps negative values and its absolute value $|M_{ZFC}(T)|$ decreases on warming. With increasing the V^{5+} doping level to $x=0.08$, T_m increases to 102 K, and the $M_{FC}(T)$ and $M_{ZFC}(T)$ behave as those of the sample with $x=0.06$. Moreover, the magnitude of the diamagnetism also increases with increasing V concentration.

As we know, V^{5+} ion itself with empty $3d$ orbits exhibits the orbital diamagnetism; however, it is believed to be weak and not to be sensitive to the external magnetic field and temperatures. The diamagnetism in samples with $x=0.04$, 0.06, and 0.08 varies obviously with temperature as shown in Fig. 3, and while applying the larger fields it turns to be a positive value, i.e., $dM/dB>0$, as discussed below, so it can be suggested that the diamagnetism does not result from the orbital diamagnetism of V^{5+} for which $dM/dB<0$ should be satisfied, although the orbital diamagnetism of V^{5+} ion itself may contribute to the negative magnetization values.

Now we take the variation of surrounding spin structures around V^{5+} ion into account for understanding the diamagnetism of the samples with $x=0.04$, 0.06, and 0.08. The V^{5+} dopant induces Mn^{3+} ion in the Mn^{4+} network of $CaMnO_3$

leading to the formation of $Mn^{3+}-O-Mn^{4+}$ DE FM interaction, setting in the $Mn^{4+}-O-Mn^{4+}$ AFM matrix. In Figs. 4(a) and 4(b), we illustrate the possible variation of spin configurations in a condition of collinear spins before and after V^{5+} doping. For $CaMnO_3$, the spins of Mn^{4+} ions have a G-type AFM structure with each spin alternatively antiparallel to that of the nearest Mn neighbors as shown in Fig. 4(a). The total spin can be represented by $G=S_1-S_2+S_3-S_4$, and its value tends to be zero in an ideal condition. When a Mn^{4+} ion is replaced by a V^{5+} ion with $s=0$, a Mn^{3+} ion is induced at the nearest Mn site, with its spin S_5 ferromagnetically coupled with S_1. As a result, the total spin becomes $G'=S_1+S_5-S_4$, as shown in Fig. 4(b), and the vector sum of the other spins beyond G' is assumed to be zero based on the character of G-type AFM structure. In fact, the ground state of spin arrangement may be canted in a system with the competition between AFM and FM couplings, as proposed by de Gennes.[11] Figure 4(c) presents the possible canted spins in an uncertain distortion angles in $CaMn_{1-x}V_xO_3$. As is well known, the average magnetization is a result of the vector sum of individual spins so the diamagnetism in $CaMn_{1-x}V_xO_3$ microscopically may be related to the magnitude and direction of $\Sigma_{i=1}^n G'_i$, where n is the number of V^{5+} ions.

To observe the response of diamagnetism on the applied magnetic field, we also measured $M_{FC}(T)$ (solid circles) and $M_{ZFC}(T)$ (empty circles), especially for the sample with $x=0.04$ which exhibits more complicated magnetic behaviors at different applied fields. The results are shown in Fig. 5. While H is increased to 0.05 T, $M_{FC}(T)$ shows diamagnetism below 44 K. As to the $M_{ZFC}(T)$ curve, a minimum appears at 70 K, but it is positive. For $H=0.5$ and 2 T, diamagnetism has been fully destroyed.

To investigate the origin of diamagnetism in $CaMn_{1-x}V_xO_3$, we have measured the temperature dependence of Young's modulus ΔE for all samples. Corresponding to the appearance of diamagnetism, ΔE exhibits an anomalous decrease with decreasing the temperature (not shown here). Such a behavior may be related to the JT distortion of $Mn^{3+}O_6$ octahedron due to the induced Mn^{3+} JT ion by V^{5+} (not a JT ion) doping at Mn^{4+} site. However, it is
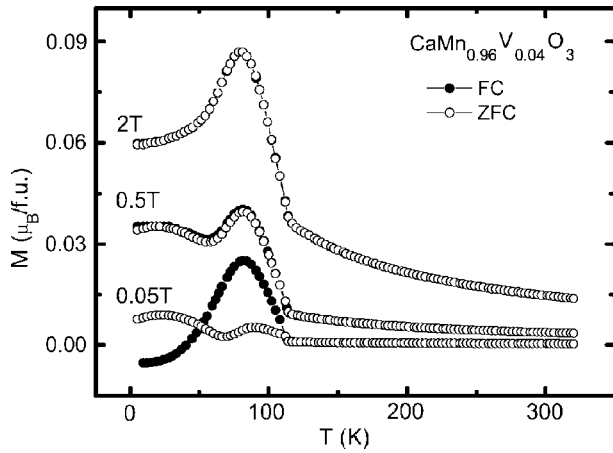
FIG. 5. The temperature dependence of $M_{FC}(T)$ (solid circles) and $M_{ZFC}(T)$ (empty circles) for the sample with $x=0.04$ at different applied fields.

insufficient to explain the diamagnetism only from the viewpoint of JT distortion, because for $Ca_{1-x}La_xMnO_3$ with $x \leq 0.1$, the concentration of Mn^{3+} JT ion is comparable with that in $CaMn_{1-x}V_xO_3$, but no diamagnetism has been observed in the $Ca_{1-x}La_xMnO_3$ compounds.[12] So the other factor has to be taken into account for understanding the diamagnetism.

As illustrated in Fig. 4(b), the Mn^{3+} ion lies between the Mn^{4+} and V^{5+} ions, which is different from that in the electron-doped $Ca_{1-x}La_xMnO_3$ with two Mn^{4+} ions occupying at the two sides of Mn^{3+} ions. This situation would lead to the variation of distortion in $Mn^{3+}O_6$ octahedron. Figure 4 gives an illustration for the $Mn^{3+}O_6$ octahedron distortion due to (d) JT effect and (e) V^{5+} substitution for Mn^{4+}. In the $Mn^{3+}O_6$ octahedron, the solid lobe denotes the orbit of e_g electron and the arrow represents the spin orientation of Mn^{3+} ion. In the electron-doped $Ca_{1-x}La_xMnO_3$, $Mn^{3+}O_6$ octahedron distorts and appears long Mn^{3+}–O bond only due to the JT effect. However, in the condition of V^{5+} substitution for Mn^{4+}, $Mn^{3+}O_6$ octahedron lies in an asymmetric environment between V^{5+} and Mn^{4+}, which would lead to an additional $Mn^{3+}O_6$ octahedron distortion besides the distortion from the JT effect. The variation of $Mn^{3+}O_6$ octahedron distortion due to V^{5+} substitution for Mn^{4+} results in the rotation of the orbit. The force generated by the orbit rotation makes the spin tilt due to the spin-orbit coupling. As a result, the vector sum of individual spins may orient along or opposite to the direction of the applied magnetic field. Macroscopically, the average magnetization exhibits positive or negative values.

D. Resistivity

Figure 6(a) shows $\rho(T)$ of $CaMn_{1-x}V_xO_3$ samples ($0.02 \leq x \leq 0.08$) at 0 and 7 T in the temperature region of 5–350 K. It indicates that ρ of the sample increases with increasing V-doping level and $\rho(T)$ of all samples behaves as semiconducting behavior in the whole measured temperature range. No metal-insulator transition is observed though the introduction of a possible DE between Mn^{3+} and Mn^{4+} due to the V^{5+} doping. The increase of ρ is suggested to originate from the increased random Coulomb potential due to the V
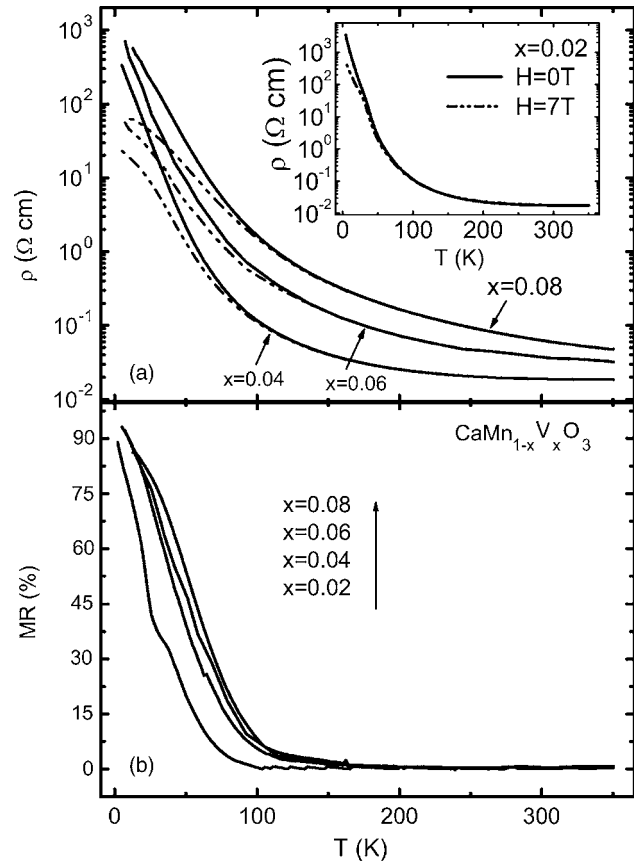

FIG. 6. (a) The temperature dependence of resistivity $\rho(T)$ and (b) MR for $CaMn_{1-x}V_xO_3$. Inset: the plot of $\rho(T)$ curve for the $x=0.02$ sample. The solid lines and the dashed lines stand for the curves at $H=0$ and $H=7$ T, respectively.

doping at Mn site, which gives rise to the localization of carriers. Moreover, a large negative MR is observed in the low temperature range below 100 K under the action of 7 T. The MR as a function of temperature is shown in Fig. 6(b). Here, the MR is defined as $\Delta\rho/\rho_0 = (\rho_0 - \rho_H)/\rho_0$, where ρ_0 is the resistivity at zero field and ρ_H is the resistivity at $H = 7$ T. The large MR at low temperatures can be related to the grain boundary effects. Similar phenomena have been reported in the perovskite manganite system.[13]

E. Thermoelectric power (TEP)

The $S(T)$ of $CaMn_{1-x}V_xO_3$ samples ($x=0.02$, 0.04, 0.06, and 0.08) at zero field is shown in Fig. 7. For $x=0.02$ sample, Fig. 7 indicates that there is a change of slope in the vicinity of magnetic transition temperature T_S^m ($=118$ K). An interesting phenomenon is that a very remarkable S peak appears at T_S^p ($=29$ K), where the absolute value of S reaches 243 μV/K. With decreasing temperature further, the absolute value of S drops rapidly below 29 K. The same trend has been observed previously for $Pr_{1-x}Sr_xMnO_3$ ($0.5 \leq x \leq 0.6$) (Ref. 14) and $La_{1-x}Ca_xMnO_3$ ($0.1 \leq x \leq 0.4$).[15]

As discussed in Ref. 15, the S peak can arise from either the phonon drag or inelastic scattering of electrons. If the sample exists a large residual ρ, which implies the dominant scattering rate τ^{-1} at low temperature comes from the inelastic scattering of electrons (i.e., $\tau^{-1} \approx \tau_{el}^{-1}$). This makes the
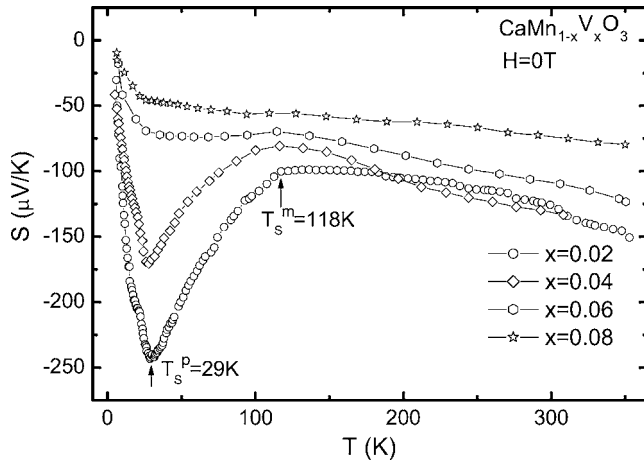
FIG. 7. The temperature dependence of $S(T)$ for $CaMn_{1-x}V_xO_3$ with x =0.02, 0.04, 0.06, and 0.08 at zero field.

phonon drag contribution a less possibility. In this instance, the scattering of electrons is a possible origin of the peak. Directly speaking, the strong inelastic scattering of electrons arises from a two level system (TLS) with energy splitting ξ at low temperature. The negative peak of S at low temperature appears at $T_S^p = \xi/4k_B$, where k_B is Boltzmann's constant and ξ expresses the difference in the energies of the crystal field split e_g levels between Mn^{3+} and Mn^{4+} ions. When an electron from Mn^{3+} ion converts into a neighboring Mn^{4+} ion, the crystal field splitting will change due to the different Mn–O bond lengths between Mn^{3+}–O and Mn^{4+}–O bond lengths. Accordingly, ξ will change as the doping content varies leading to the shift of the peak position T_S^p.[15] But for the present system, a nearly doping-independent T_S^p is observed and it only shows the decrease of the peak value in the vicinity of T_S^p, as shown in Fig. 7. Thus there is no enough evidence to interpret the source of the peak by the scattering of electrons. The effect of phonon drag should be more reasonable to explain the origin of the peak. Since for $CaMn_{1-x}V_xO_3$ samples $(0.02 \leqslant x \leqslant 0.08)$, $\rho(T)$ behaves as semiconductorlike transport behavior in the whole measured temperature range, and electron-phonon scattering at low temperature dominates the scattering rate τ^{-1} (i.e., $\tau^{-1} \approx \tau_{el\text{-}ph}^{-1}$). Due to the electron-phonon interaction, the phononic diffusion flow will drive the electrons to move from hot side to cold side. It can be expected that the V dopant will be the center of phononic scattering inside the $Mn^{3+}O_6$ octahedron resulting in the decrease of the electron-phonon scattering interaction. From Fig. 7, we can clearly see that with increasing V doping level, the height of the peak in the vicinity of T_S^p decreases, implying that phonon-drag effect reduces after V doping. This reduction of phonon-drag effect results from the phononic high-frequency vibrations of the V dopants, which prevents the phonon scattering to the electrons.

In addition, with increasing V-doping level, the absolute $S(T)$ in the vicinity of T_S^m also decreases gradually as plotted in Fig. 7. We suggest that this can originate from the combined effect due to the increased DE FM interaction between Mn^{3+} and Mn^{4+}, which leads to the reduction of the spin entropy [the decrease of the absolute $S(T)$], and exceeds the

increasing of an additional spin entropy because of the diamagnetism generating by the orbit rotation, which results in the increase of the absolute $S(T)$. Namely, the value of absolute S is extremely sensitive to the Mn^{3+} content. The Mn^{3+} content increases with increasing V-doping level giving rise to smaller value of absolute $S(T)$ in the vicinity of T_S^m.

As to the steep decrease of absolute $S(T)$ in the low temperature region below T_S^p with increasing V doping as shown in Fig. 7, it is proposed to come from the carrier localization effect due to the gradual suppression of carrier hopping by V doping at low temperature. Its origin will be further explained below.

Figure 8 shows the temperature-dependent $S(T)$ both in the absence $(H=0$ T$)$ and presence $(H=3$ T$)$ of magnetic field for the samples with $0.02 \leqslant x \leqslant 0.08$. It is found that application of magnetic field induces reduction of absolute $S(T)$ at almost the same temperature T_S^p as shown in Figs. 8(a)–8(d). On one hand, this attributes to the fact that magnetic entropy may be strongly decreased only around T_S^p.[16] That is to say, when an external field exists, magnetic disorder is expected to become weaker due to the accordant spin arrangement, so that magnetic entropy is reduced with increase of magnetic field. On the other hand, the additional spin entropy because of the diamagnetism generated by the orbit rotation will reduce in applied fields, which is ascribed to the weakness of spin-orbit coupling. In brief, as discussed above in the section of magnetic property, the force generated by the orbit rotation makes the spin tilt because of the spin-orbit coupling. However, as the external field arises, the canted spins may orient along or opposite to the direction of the external field. As a result, the orbital angular momentum is suppressed in the magnetic configuration. Such a suppression implies that the spin-orbit coupling weakens with applied field.

It is worth noting that in the high temperature region of $T > T_S^m$ for the samples with $x \geqslant 0.04$, since the thermal disorder becomes too large, S becomes independent of magnetic field as plotted in Figs. 8(b)–8(d). In the low temperature region of $T < T_S^p$ for the samples with $x \leqslant 0.04$, the magnetic entropy is already frozen by the magnetic exchange coupling which also gives rise to a nearly field-independent $S(T)$ as shown in Figs. 8(a) and 8(b). Figures 8(e)–8(h) indicate the thermal variation of magnetothermoelectric power (MTEP). The MTEP is expressed as $\Delta S/S_0 = |S_0 - S_H|/S_0$, where S_0 is the TEP at zero field and S_H is the TEP at 3 T. Especially for the samples with $x=0.06$ and 0.08, MTEP increases remarkably and up to 60% at low temperatures, indicating the magnetic entropy is suppressed dramatically.

In the following, we will focus on analyzing the transport mechanism of $CaMn_{1-x}V_xO_3$ samples combined with ρ and S data.

1. High temperature ($T > T_S^m$) transport mechanism

In the high temperature region of $T > T_S^m$, it is found that both $S(T)$ and $\rho(T)$ follow the adiabatic small polaron conduction (SPC) mechanism. In the framework of SPC model, $\rho(T)$ can be described by
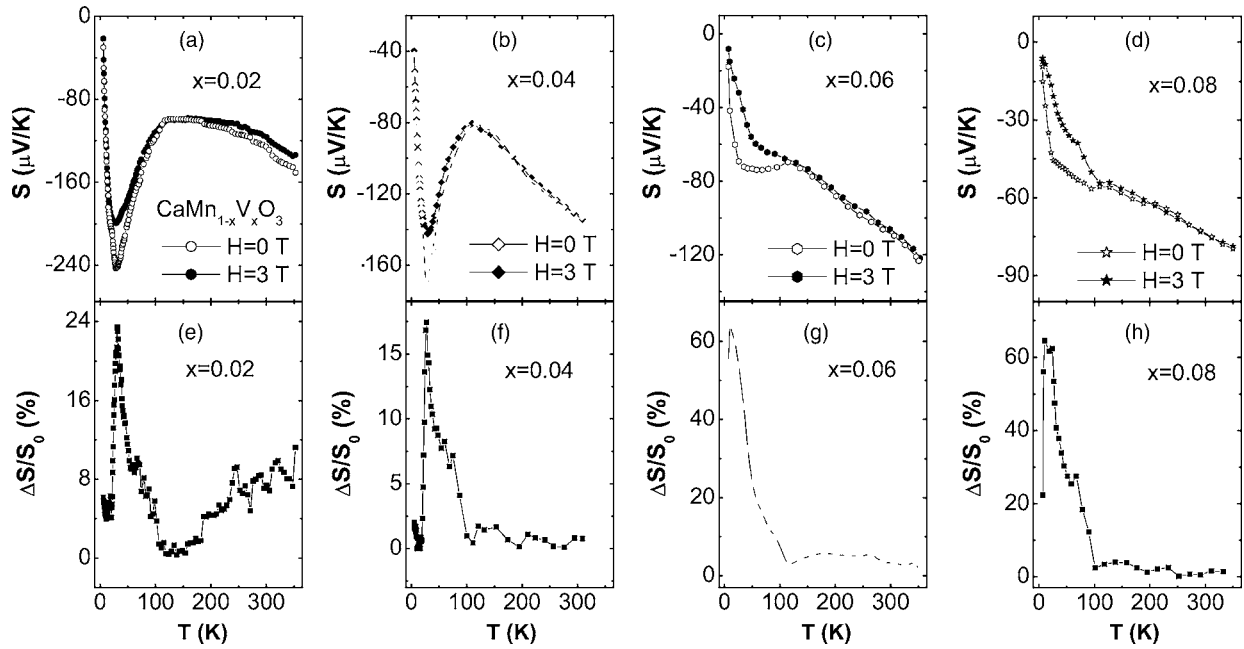
FIG. 8. [(a)–(d)] The temperature dependence of $S(T)$ and [(e)–(h)] the temperature dependence of magnetothermoelectric power at $H=0$ and 3 T, respectively.

$$\rho = \rho_0 T \exp(E_\rho/k_B T), \tag{1}$$

where E_ρ is the activation energy obtained according to the fitting of the $\rho(T)$ data.[17]

The values of activation energy E_ρ are listed in Table I at zero field and external magnetic field, respectively. For SPC, $S(T)$ should be described by the following equation:[17]

$$S(T) = k_B/e(E_S/k_B T + \alpha), \tag{2}$$

where k_B is Boltzmann's constant, e is the electron's charge, E_S is the activation energy obtained according to the fitting of the $S(T)$ data, and α is a sample-dependent constant, which is associated with the spin and the mixing entropy.[18] The curves of S vs $1000/T$ for the samples are plotted in Figs. 9(a), 9(c), and 9(e) for $H=0$ and Figs. 9(b), 9(d), and 9(f) for $H=3$ T, respectively. The scatter symbols correspond to the experimental data and the solid lines denote the fitted results according to Eq. (2). The parameter χ^2 (reduced chi-square value of fit) related to the quality of the fit is also denoted in Fig. 9. The fitting values of E_S are listed in Table I, which show that E_S gradually decreases and E_ρ increases with increasing V-doping level. Moreover, the magnitude of E_S is much smaller than that of E_ρ, which is the character of

SPC. In short, in the framework of the SPC model, E_ρ is the sum of the activation energy needed for the creation of the carriers and activating the hopping of carriers, and E_S is the energy required to activate the hopping of carriers. Hence, E_S is much smaller than E_ρ. In addition, based on E_ρ and E_S, both the polaronic hopping energy $W_H = E_\rho - E_S$ and the polaronic formation energy $E_p = 2W_H$ can be obtained as denoted in Table I.

Figure 10(a) shows E_ρ and E_S obtained from $\rho(T)$ and $S(T)$ for $CaMn_{1-x}V_xO_3$. As V doping increases, E_ρ rises monotonously at zero field while E_S decreases slowly. Accordingly, E_p increases with increasing V-doping level. Firstly, the result will be attributed to the extra introduction of Mn^{3+} ions by V-doping level. Because the Mn^{3+} ion is associated with a local JT distortion, additional Mn^{3+} sites due to V substitution lead the carriers to be localized. Previously it has been reported that the Mn^{3+} concentration is closely related to E_p, which exhibits a strong increase of E_p for the lattice polaron with increasing Mn^{3+} concentration.[19] Secondly, the lattice strain due to V doping can contribute to the increase of E_p. Since the size of V ion is different from that of the Mn ion, V doping is expected to affect the bond angles and bond

TABLE I. Both E_ρ and E_S are activation energies calculated by fitting $\rho(T)$ and $S(T)$ curves according to SPC model for the samples with V-doping level of $x=0.02$, 0.04, 0.06, and 0.08 in the high temperature region in the absence and presence of magnetic field. W_H is the hopping energy of the small polaron in a given direction. E_p is the formation energy of the small polaron. "$\pm$" expresses the error which forms by fitting $\rho(T)$ and $S(T)$ data.

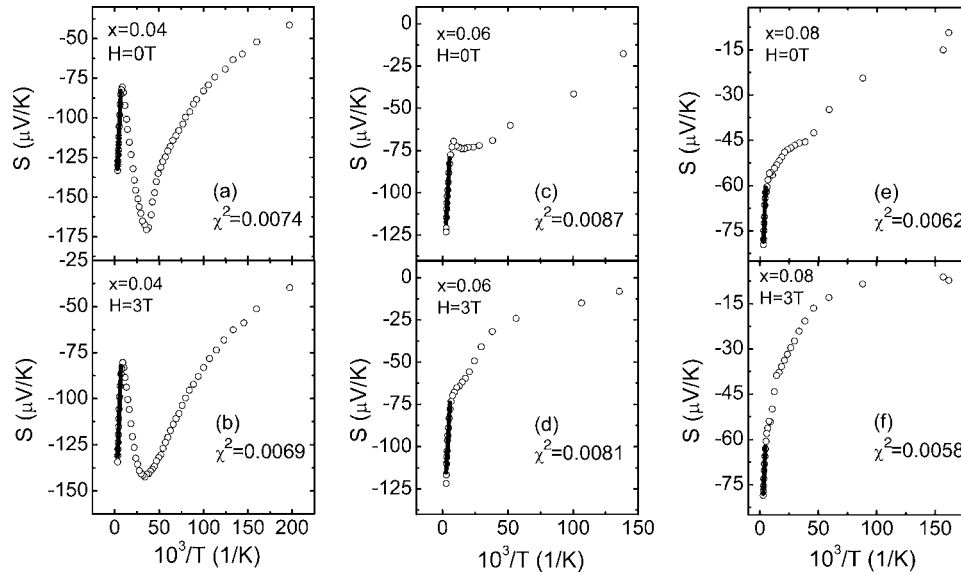| Parameter V content	E_ρ (meV)			E_s (meV)		W_H/k_B (K)		E_p (meV)	
	0 T	3 T	7 T	0 T	3 T	0 T	3 T	0 T	3 T
$x=0.02$	36.3 ± 0.1	35.1 ± 0.2	34.2 ± 0.1	7.8 ± 0.2	6.9 ± 0.1	392	388	57.0	56.4
$x=0.04$	37.2 ± 0.2	36.0 ± 0.1	35.3 ± 0.1	6.4 ± 0.1	5.8 ± 0.1	424	416	61.6	60.4
$x=0.06$	54.8 ± 0.2	53.2 ± 0.2	51.6 ± 0.1	6.0 ± 0.1	5.4 ± 0.1	672	658	97.6	95.6
$x=0.08$	71.2 ± 0.1	68.5 ± 0.1	67.8 ± 0.2	4.5 ± 0.1	4.1 ± 0.1	918	887	133.4	128.8

FIG. 9. [(a), (c), and (e)] The plot of S vs $1000/T$ in the high temperature region at zero field and [(b), (d), and (f)] at $H=3$ T. The solid lines of (a), (c), and (e) and (b), (d), and (f) correspond to the fitting by SPC model. The parameter χ^2 (reduced chi-square value of fit) represents the quality of the fit.

lengths of the neighboring $Mn^{3+}-O-Mn^{4+}$ channels. This local lattice strain due to the cation size difference lifts the degeneracy of the e_g states of Mn ion. Consequently, the lower e_g state serves as a trapping level,[20] which favors the

FIG. 10. (a) Activation energies of resistivity (E_ρ) and TEP (E_S) for $CaMn_{1-x}V_xO_3$ ($0 \leq x \leq 0.08$) at zero field obtained from the SPC fitting in Fig. 9. E_ρ data of $CaMn_{1-x}Ru_xO_3$ is included for comparison, which comes from the reported data (Ref. 21). (b) TEP at 300 K ($S_{300\ K}$) of $CaMn_{1-x}V_xO_3$ ($0 \leq x \leq 0.08$) is plotted to estimate the Mn valence. $S_{300\ K}$ of $CaMnO_3$ originates from the reported data (Ref. 24). The dotted line is a guide to the eyes.

increase of E_p. As to the slight reduction of E_S, this can be attributed to the decreasing of the width for the polaron band gap.

For comparison, E_ρ of $CaMn_{1-x}Ru_xO_3$ (Ref. 21) is also plotted in Fig. 10(a). The magnitude of E_ρ is close between V^{5+} and Ru^{5+} due to the same valence. The Mn^{3+} ions induced by these cations enhance the local JT distortion in the sample and make the system form small polarons. The dopants play the role of scattering centers inside the $Mn^{3+}O_6$ octahedron. Additionally, the local lattice strain for the dopants is also very important as discussed above. Therefore, E_ρ should increase with increasing the doping level. Nevertheless, for Ru-doped sample, interestingly, E_ρ decreases with increasing Ru-doping level. It is believed that the e_g^0 states of Ru^{5+} can participate in the band formation by coupling with Mn^{3+} (e_g^1) and make the band become broader. As Ru-doping concentration reaches a certain percentage, the effect will become dominant, which decreases E_ρ rather than increases it.[21]

In addition, from Table I, it is clearly seen that the applied field reduces the activation energy E_S and E_ρ. This may be due to the delocalization e_g^1 electron of Mn^{3+} ions.[22] In other words, the carriers are polarons at zero field, but are delocalized carriers in the external field at the same temperature, which leads to the increase of conductivity. The decrease of W_H in the applied field implies an increase of the polaronic radius with field,[18] which is also supported from the following relationship due to Mott and Davis:[17]

$$W_H \propto \frac{e^2}{4\varepsilon_0 r_p}, \tag{3}$$

where ε_0 reflects the change in the Fermi energy and r_p is the polaronic radius. Evidently, the change of W_H is certainly opposite to r_p with field.

Figure 10(b) indicates S value at 300 K for $CaMn_{1-x}V_xO_3$. It is well known that the $S_{300\ K}$ value of the high-T_C cuprates shows a systematic change related to the

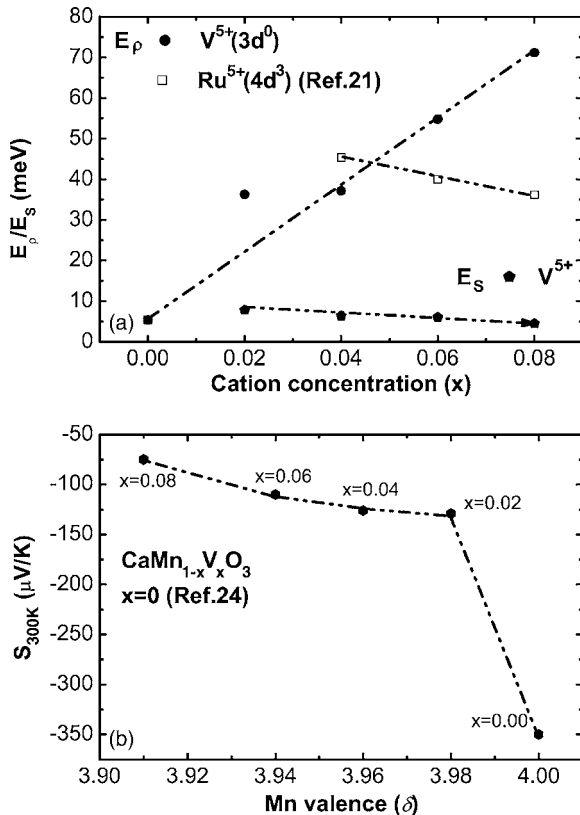TABLE II. The fitting parameters of $S(T)$ and $\rho(T)$ curves according to the three-dimension VRH model in the low temperature regions in the absence and presence of magnetic field. T_0 denotes the characteristic temperature and A is a fitting parameter for $S(T)$ in the low temperature region. "$\pm$" stands for the error which forms by fitting $\rho(T)$ and $S(T)$ data.

Parameter V content	$(T_0)^{1/4}$ (K$^{1/4}$)			A (μV K$^{-3/2}$)	
	0 T	3 T	7 T	0 T	3 T
$x=0.02$	6.94±0.02	5.12±0.01	2.79±0.02	100.6±0.2	96.2±0.1
$x=0.04$	11.73±0.01	8.61±0.02	3.15±0.01	43.4±0.1	41.9±0.2
$x=0.06$	12.64±0.01	10.27±0.01	4.23±0.01	24.3±0.1	22.6±0.1
$x=0.08$	13.18±0.02	12.46±0.01	6.87±0.02	13.5±0.1	11.8±0.1

carrier density.[23] Also, as discussed above, the value of $S_{300\,K}$ directly depends on the carrier concentration, so that $S_{300\,K}$ is sensitive to the Mn valence.[8] Hence, $S_{300\,K}$ can be used as a measure of the valence of Mn ions in this system. The absolute $S_{300\,K}$ is the largest for CaMnO$_3$ (350 μV/K);[24] $S_{300\,K}$ decreases as the Mn valence decreases. The large negative S at room temperature makes the free sample and slightly V-doped sample generate n-type legs for a thermoelectric device as recently reported in Ca$_{1-x}$La$_x$MnO$_3$ manganites.[25]

2. Low temperature ($T < T_S^p$) transport mechanism

In the low temperature region of $T < T_S^p$, Mott and Davis' three dimensional (3D) variable-range-hopping (VRH) model matches the experimental data better for both $\rho(T)$ and $S(T)$. In the framework of 3D VRH model, $\rho(T)$ meets the following equation:[17]

$$\rho(T) = \rho_0 \exp[(T_0/T)^{1/4}], \qquad (4)$$

where T_0 is a characteristic temperature which is related to the density of states in the vicinity of the Fermi energy, $N(E_F)$, and the localization length ζ, i.e., $k_B T_0 \approx 21/[k_B N(E_F)\zeta^3]$. The values of T_0 are listed in Table II at zero field and external field, respectively.

For 3D VRH model, $S(T)$ in the low temperature region ($T < T_S^p$) meets the following relationship:[26,27]

$$|S| = A(T)^{1/2} + B, \qquad (5)$$

where A is a factor determined by $N(E_F)$ and B is a constant. The complete derivation for these parameters of Eq. (5) can be found in literature.[28] The curves of S vs $T^{1/2}$ for the samples are plotted in Figs. 11(a) and 11(c) at $H=0$ T and Figs. 11(b) and 11(d) at $H=3$ T, respectively. The parameter χ^2 of the fitting quality is also plotted in Fig. 11. The fitting parameter A is listed Table II.

From Table II, it is found that T_0 increases and A decreases with increasing V-doping level, implying the strengthened localization of the carrier if the variation of $N(E_F)$ in the vicinity of Fermi surface is not considered. In addition, it is found that the applied magnetic field reduces the values of T_0 and A, which is attributed to the delocalization of the carrier caused by the applied field.

F. Thermal conductivity

The $\kappa(T)$ of CaMn$_{1-x}$V$_x$O$_3$ samples ($0.02 \leq x \leq 0.08$) at zero field is shown in Fig. 12. For the sample with $x=0.02$, it seems to be consistent with the usual heat transport. However, it also behaves as an anomalous feature. Speaking di-
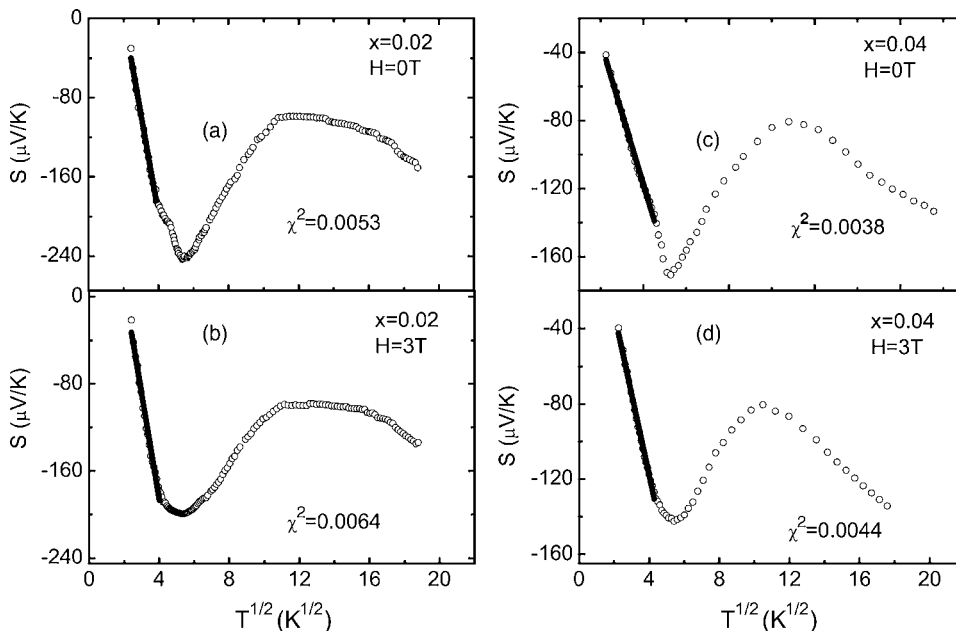
FIG. 11. [(a) and (c)] The plot of S vs $T^{1/2}$ for CaMn$_{1-x}$V$_x$O$_3$ ($x=0.02$ and 0.04) in the low temperature region at zero field and [(b) and (d)] at $H=3$ T. The solid lines are the fitting data according to the VRH model. The parameter χ^2 denotes the quality of the fit.
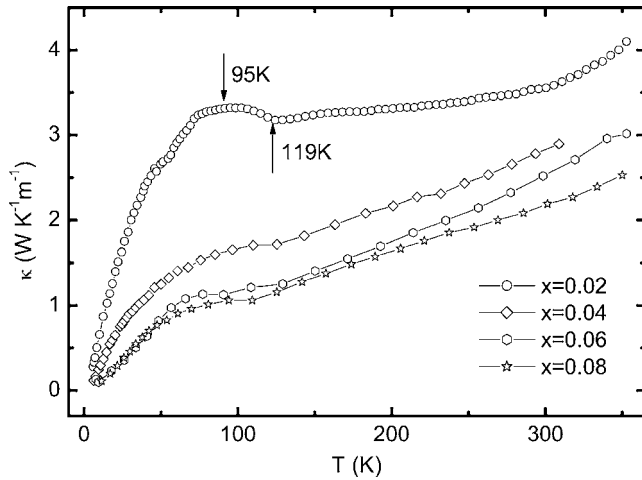
FIG. 12. The temperature dependence of the measured total κ of $CaMn_{1-x}V_xO_3$.

rectly, the $\kappa(T)$ decreases with increasing temperatures between the peak temperature (=95 K) and magnetic transition temperature (T_k^m=119 K), implying that an unusual additional scattering mechanism may be active above 95 K besides the phonon-phonon Umklapp scattering. The additional scattering is suggested to originate from the scattering of the dynamic local $Mn^{3+}O_6$ JT distortion to the phonon because of the introduction of Mn^{3+} JT ions due to the partial substitution of V^{5+} (not a JT ion) for Mn^{4+} (not a JT ion).[29] Figure 12 shows that κ decreases and the low temperature κ peak is strongly suppressed with increasing V-doping level. This kind of variation is attributed to the enhanced scattering of the local $Mn^{3+}O_6$ JT lattice distortion to the phonon due to the introduction of more Mn^{3+} ions. In addition, the en-

hanced disorder induced by V doping also scatters the phonon, which leads to the decrease of κ. Therefore, the decrease of κ with increasing V doping is suggested to come from the combined effect of the scattering of the $Mn^{3+}O_6$ JT distortion and the disorder to the phonon.

In order to investigate the magnetothermal conductivity of the sample, the $\kappa(T)$ under the action of the applied magnetic field is measured. The $\kappa(T)$ of the sample with x =0.02, 0.04, 0.06, and 0.08 at H=3 T is shown in Figs. 13(a), 13(c), 13(e), and 13(g), respectively. For comparison, the $\kappa(T)$ of all samples at H=0 T is also plotted in Figs. 13(a), 13(c), 13(e), and 13(g). Similar to MTEP, $\kappa(T)$ is obviously suppressed only near the magnetic compensation point in the applied field. There is no doubt that $\kappa(T)$ displays a clear identifying characteristic of the influence of spins on the heat transport. It is not the self-localization nature of the polarons that impedes the energy flow associated with the charge carriers. Considering as the carrier contribution to the heat flow, which is only a very tiny fraction of the total heat flow, so that the carrier contribution is ultimately ignored. If the decrease of $\kappa(T)$ in the external field is attributed to the contribution of spin fluctuations, which is also illogical. Since the external magnetic field tends to suppress the spin fluctuations which can scatter the phonon.[30] Consequently, $\kappa(T)$ should rise in the applied field, which is an inverse of the present results. Therefore, it is necessary to search exceptive mechanism to explain the abnormal phenomenon.

Here, we ascribe the decrease of $\kappa(T)$ under magnetic field to the contribution from spin-phonon coupling.[31] The measurements of $\kappa(T)$ in a magnetic field make this point quite clear. As we know, the magnitude of phononic vibrant
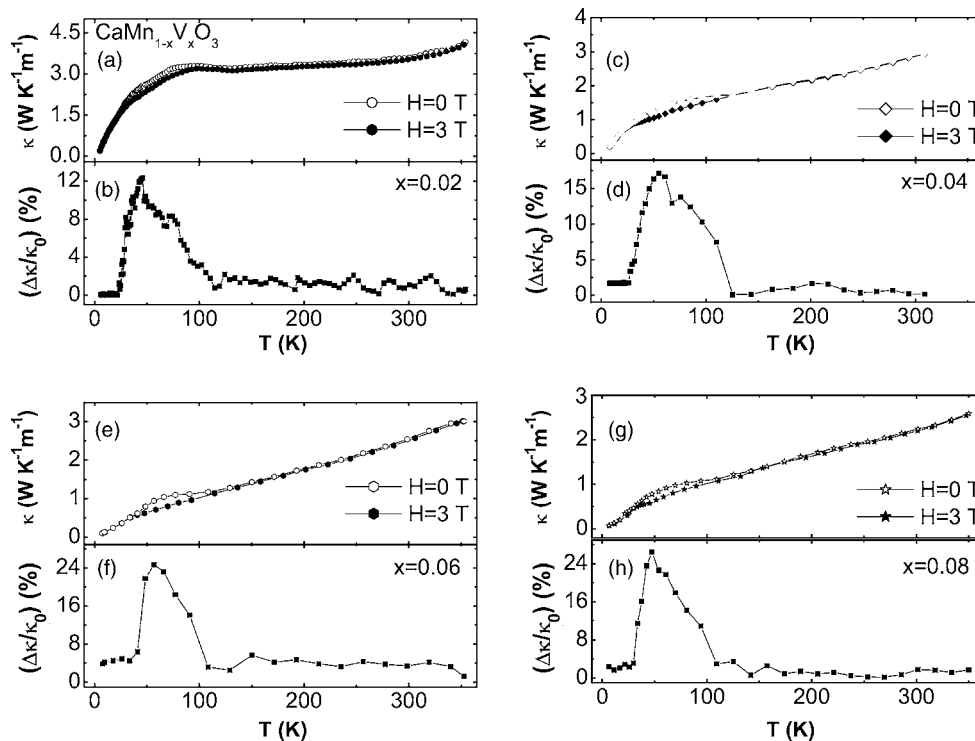

FIG. 13. [(a), (c), (e), and (g)] The temperature dependence of $\kappa(T)$ and [(b), (d), (f), and (h)] magnetothermal conductivity at H=0 and H=3 T, respectively.
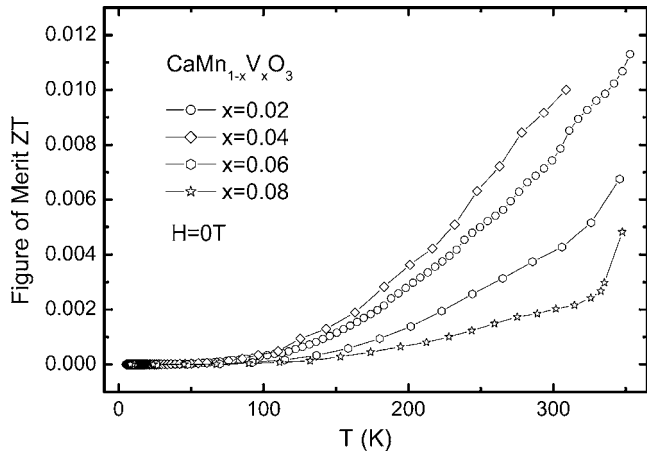
FIG. 14. The temperature dependence of figure of merit for $CaMn_{1-x}V_xO_3$ at zero field.

frequency usually plays a very important role in determining heat transport behavior. In the presence of magnetic field, spin arrangement becomes more accordant and the intensity of phonon scattering enhances. Namely, in the spin-order state, the phononic vibrant frequency becomes weaker due to the stronger spin-phonon coupling under magnetic field impeding the heat flow of phonons, which gives rise to the reduction of κ. Figures 13(b), 13(d), 13(f), and 13(h) shows the thermal variation of magnetothermal conductivity (MTC). The MTC is denoted as $\Delta\kappa/\kappa_0 = (\kappa_0 - \kappa_H)/\kappa_0$, where κ_0 and κ_H is the thermal conductivity at zero field and 3 T magnetic field, respectively. The curves $\Delta\kappa(T)/\kappa_0(T)$ clearly reflects the intensity of spin-phonon coupling. Due to the appearance of spin-phonon coupling, the mean free path of the phonon (l_{ph}) can split into two parts, viz., nonmagnetic (l_{nm}) and magnetic (l_m) parts as $1/l_{ph} = 1/l_{nm} + 1/l_m$, where l_{nm} expresses the mean free path determined by phonon-phonon Umklapp scattering, *etc.*, and l_m represents that determined by spin-phonon coupling. In fact, this kind of spin correlation is also reflected by the measurement of magnetic property. In detail, the magnitude of magnetization increases with increasing applied field, meanwhile, diamagnetism is destroyed when the applied magnetic field exceeds to 0.05 T, and FM interaction enhances. Consequently, the spin correlation distinctly increases under higher magnetic field.

G. Figure of merit

Based on the data of $\rho(T)$, $S(T)$, and $\kappa(T)$, the dimensionless thermoelectric figure of merit $Z = S^2/\rho\kappa$ at zero field for all samples is calculated. The obtained result is shown in Fig. 14. It indicates that the *ZT* values tend to increase with increasing temperatures. For the sample with $x=0.04$, its *ZT* value reaches 0.01 at room temperature, which almost approaches the *ZT* value (0.032) observed in $NaCo_2O_4$.[32] Therefore, the slightly V-doped manganites may be good candidates for thermoelectric materials.

In brief, from the above results, it is found that the doped V^{5+} ion plays a crucial role to determine the diamagnetism, transport, MTEP, and MTC in electron-doped $CaMn_{1-x}V_xO_3$ manganites. The observed results are strongly related to the characteristic of the V^{5+} ion because the large MTEP and

MTC only appear in the region of anomalous diamagnetism. In the applied field, the variation of both the spin-orbit coupling and the spin-phonon coupling can be found by $S(T)$ and $\kappa(T)$ measurements. Such changes also reflect the special role of V^{5+} ion. At the same time, it can also help us to improve our understanding to other complex systems.

IV. CONCLUSION

In summary, we have systematically investigated the influence of the V doping on $M_{FC}(T)$, $M_{ZFC}(T)$, $\rho(T)$, $S(T)$, and $\kappa(T)$ of $CaMn_{1-x}V_xO_3$ $(0.02 \leq x \leq 0.08)$ samples. As $x > 0.02$, an anomalous diamagnetism has been observed. The diamagnetism is also enhanced after the V^{5+} substitution for Mn^{4+}. It is suggested that the diamagnetism results from the spin tilting generated by the orbit rotation. All samples behaves as SPC mechanism in the high temperature region and VRH mechanism in the low temperature range based on the analysis of $S(T)$ and $\rho(T)$ data. The large S peak is attributed to the effect of phonon drag. In addition, the observed obvious MTEP and MTC in the temperature region exhibiting an anomalous diamagnetism is suggested to originate from the effect of the field on spin-orbital coupling and spin-phonon coupling, respectively. Interestingly, a large *ZT* value for the sample with $x=0.04$ at the room temperature is observed, which may imply that the slightly V-doped manganites may be good candidates for thermoelectric materials.

[1]S. Jin, T. H. Tiefel, M. McCormack, R. A. Fastnacht. R. Ramesh, and L. H. Chen, Science **264**, 413 (1994); A. Asamitsu, Y. Moritomo, Y. Tomioka, T. Arima, and Y. Tokura, Nature (London) **373**, 407 (1995); R. von Helmolt, J. Wecker, B. Holzapfel, L. Schultz, and K. Samwer, Phys, Phys. Rev. Lett. **71**, 2331 (1993).

[2]C. Zener, Phys. Rev. **82**, 403 (1951); P.-G. de Gennes, *ibid.* **118**, 141 (1960).

[3]J. B. Goodenough, Phys. Rev. **100**, 564 (1955).

[4]A. J. Millis, P. B. Littlewood, and B. I. Shraiman, Phys. Rev. Lett. **74**, 5144 (1995).

[5]J. M. de Teresa *et al.*, Nature (London) **386**, 256 (1997).

[6]P. Mandal and S. Das, Phys. Rev. B **56**, 15073 (1997); S. Roy and N. Ali, J. Appl. Phys. **89**, 7425 (2001); G. T. Tan, S. Dai, P. Duan, Y. L. Zhou, H. B. Lu, and Z. H. Chen, Phys. Rev. B **68**, 014426 (2003).

[7]H. Chiba, M. Kikuchi, K. Kasuba, Y. Muraoka, and Y. Syono, Solid State Commun. **99**, 499 (1996); I. O. Troyanchuk, N. V. Samsonenko, H. Szymezak, and A. Nabialek, J. Solid State Chem. **131**, 144 (1997); C. Martin, A. Maignan, F. Damay, M. Hervieu, and B. Raveau, *ibid.* **134**, 198 (1997).

[8]B. Raveau, A. Maignan, C. Martin, and M. Hervieu, Mater. Res. Bull. **35**, 1579 (2000).

[9]H. C. Nguyen and J. B. Goodenough, Phys. Rev. B **52**, 324 (1995); Y. Ren, T. T. M. Palstra, D. I. Khomskii, E. Pellegrin, A. A. Nugroho, A. A. Menovsky, and G. A. Sawatzky, Nature (London) **396**, 441 (1998).

[10]C. V. Ramana, O. M. Hussain, B. Srinivasulu Naidu, and P. J. Rcddy, Thin Solid Films **305**, 219 (1997); M. Ghanashyam Krishna, Y. Debauge, and A. K. Bhattacharya, *ibid.* **312**, 116 (1998).

[11]P.-G. de Gennes, Phys. Rev. **118**, 141 (1960).

[12]A. L. Cornelius, B. E. Light, and J. J. Neumeier, Phys. Rev. B **68**, 014403 (2003).

[13] A. Gupta *et al.*, Phys. Rev. B **54**, 15629 (1996); A. de Andres, M. Garcia-Hernandez, and J. L. Martinez, *ibid.* **60**, 7328 (1999).

[14] B. Fisher, L. Patlagan, and G. M. Reisner, Phys. Rev. B **54**, 9359 (1996); J. Hejtmanek, Z. Jirak, E. Pollert, D. Sedmidubsky, A. Strejc, C. Martin, A. Maignan, and V. Hardy, J. Appl. Phys. **91**, 8275 (2002).

[15] R. Mahendiran, S. K. Tiwary, and A. K. Raychaudhuri, Solid State Commun. **98**, 701 (1996).

[16] Y. Y. Wang, N. S. Rogado, R. J. Cava, and N. P. Ong, Nature (London) **423**, 425 (2003).

[17] N. F. Mott and E. A. Davis, *Electronic Processes in Non-Crystalline Materials* (Clarendon, Oxford, 1971).

[18] M. Jaime, M. B. Salamon, M. Rubinstein, R. E. Treece, J. S. Horwitz, and D. B. Chrisey, Phys. Rev. B **54**, 11914 (1996).

[19] J. M. De Teresa, K. Dorr, K. H. Muller, L. Schultz, and R. I. Chakalova, Phys. Rev. B **58**, 5928 (1998).

[20] K. Ghosh, S. B. Ogale, R. Ramesh, R. L. Greene, T. Venkatesan, K. M. Gapchup, R. Bathe, and S. I. Patil, Phys. Rev. B **59**, 533 (1999).

[21] L. Pi, S. Hébert, C. Martin, A. Maignan, and B. Raveau, Phys. Rev. B **67**, 024430 (2003).

[22] A. Banerjee, S. Pal, S. Bhattacharya, B. K. Chauhuri, and H. D. Yang, Phys. Rev. B **64**, 104428 (2001).

[23] S. D. Obertelli, J. R. Cooper, and J. L. Tallon, Phys. Rev. B **46**, 14928 (1992).

[24] A. Maignan, C. Martin, F. Damay, B. Raveau, and J. Hejtmanek, Phys. Rev. B **58**, 2758 (1998).

[25] I. Matsubara, R. Funahashi, T. Takeuchi, S. Sodeoka, T. Shimizu, and K. Ueno, Appl. Phys. Lett. **78**, 3627 (2001).

[26] I. P. Zvyagin, Phys. Status Solidi B **58**, 443 (1973).

[27] H. Overhof, Phys. Status Solidi B **67**, 709 (1975).

[28] I. P. Zvyagin, *Hopping Transport in Solids*, edited by M. Pollak and B. Shklovskii (North-Holland, Amsterdam, 1991), Vol. 28, Chap. 5, pp. 143–174.

[29] M. Matsukawa *et al.*, Phys. Rev. B **67**, 104433 (2003).

[30] J. Hejtmanek, Z. Jirak, M. Marysko, C. Martin, A. Maignan, M. Hervieu, and B. Raveau, Phys. Rev. B **60**, 14057 (1999).

[31] M. R. Ibarra, P. A. Algarabel, C. Marquina, J. Blasco, and J. Garcia, Phys. Rev. Lett. **75**, 3541 (1995).

[32] I. Terasaki, *Proceedings of the 18th International Conference on Thermoelectrics (ICT'99), Baltimore, 1999* (IEEE, Piscataway, NJ, 2000), p. 569.